International Forum on Aeroelasticity and Structural Dynamics
IFASD 2024
17-21 June 2024, The Hague, The Netherlands

CO-DESIGN OF THE AEROELASTIC WING PARAMETERS AND THE FLUTTER CONTROL LAW

Zsombor Wermeser[1], Béla Takarics[1], Bálint Vanek[1]

[1]HUN-REN Institute for Computer Science and Control
H - 1111 Budapest, Kende utca 11-13. ,Hungary
wermeser@sztaki.hu, takarics@sztaki.hu, vanek@sztaki.hu

Keywords: flutter control, co-design

Abstract: In an aircraft design process, the initial airframe design is iteraively refined going back and forth between structural and control design. Instead of this iteration, the simultaneous optimization of the structure and the control laws would be advantageous. This paper presents a co-design for a flutter suppression controller for a simple rectangular flexible wing. The wing is parametrized by seven geometric and structural variables. The controller is based on output feedback, whose parameters are simultaneously optimized with the structure. A solution to the same co-design problem was already proposed by Filippi et. al. (2018) [1] by directly synthesizing the optimal control input along with the optimal parameters. In this paper, a solution is presented for the design of a control law instead of the control signals. The paper uses the model parameterization by Filippi to achieve comparable results. The behavior of the wing is evaluated by time domain simulations. The objective of the co-design method takes into consideration the maneuverability, comfortability, and control cost of the wing for two types of wind gusts. The results prove that the output feedback, instead of the optimal control inputs created by Filippi optimization, works more efficiently in a co-design framework. Thus, the sensor-based flutter suppression is successfully applicable for co-design purposes.

1 INTRODUCTION

In engineering practices, the application of control design has become widespread across a diverse range of systems. Typically, this entails a systematic approach where the initial steps involve the creation of a structural model followed by the design and implementation of a suitable controller for the system. However, conventional model development strategies often entail a fixed sequence of phases, thereby constraining the system between steps and limiting opportunities for design refinement.

To optimize the overall performance of a complex system, there is an increasing need for the simultaneous design of interconnected phases. This approach, known as co-design, involves the integrated optimization of structural models and their corresponding controls, which can be beneficial for the aircraft design process. Controlling aeroelastic phenomena such as flutter in flexible aircraft systems presents a significant engineering challenge. Flutter, characterized by self-excited structural oscillations arising from aerodynamic forces, poses a potential threat to the stability and safety of aircraft operations. Recently, the use of active control systems to mitigate flutter was investigated in the literature [2–4]. Such a control system can increase the flutter speed to expand the safe flight envelope.

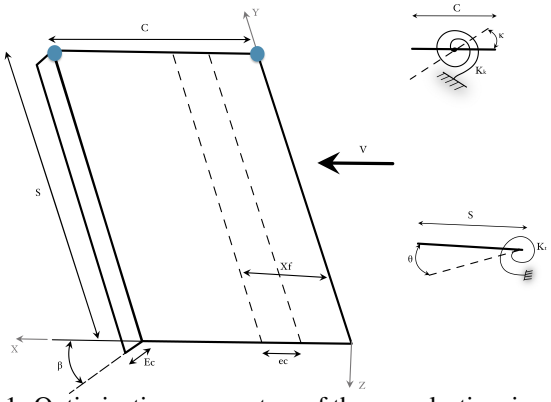

Figure 1: Optimization parameters of the aeroelastic wing [8]

The co-design has received limited attention in scientific literature. In a study by Denieul et al. [5], the control surface sizes of an aircraft are optimized using an H_∞ baseline control strategy. Faisse et al. [6] developed a framework to enhance both the structure and control system of an aeroelastic wing with flutter control. They modeled the airfoil structure as a clamped beam with a two-cell thin-walled cross-section, using five thickness parameters for optimization, and applied an H_∞ control to mitigate flutter. Nguyen et al. [7] utilized a co-design approach to simultaneously minimize the vertical tail while optimizing longitudinal and lateral control laws and engine allocations. Filippi et al [1] design seven aeroelastic wing parameters of a simple rectangular flexible wing with a flutter suppression control. They evaluates the method by time domain simulations. The method relies on a Direct Transcription approach to determine optimal control surface angles at specific time instances, thereby stabilizing the wing.

This paper aims to optimize both the control law and structural parameters of a simple flexible wing model simultaneously. Following a similar model and objective as outlined in [1], we employ an evaluation method that facilitates comparative analysis. Our method involves utilizing output feedback control from various sensor signals. The primary objective is to demonstrate the feasibility of simultaneous optimization, with the goal of tuning a controller to suppress flutter phenomena and stabilize the wing. We evaluate the effectiveness of our approach by comparing our results with those obtained by Filippi et al., which are accessible in [1].

The rest of the paper is structured as follows. In Section 2, we present the modeling approach for the simplified flexible wing. Section 3 provides a detailed discussion of the control laws. Section 4 outlines the objective function and the optimization method employed. The results are presented in Section 5. Finally, Section 6 presents the concluding remarks.

2 MATEMATICAL MODELLING OF THE AEROELASTIC SYSTEM

In this paper, we consider the geometric and structural characteristics of an aeroelastic wing. The matematical model of the wing is given as a function of model parameters and is taken from [8]. Filippi's research is also based on this wing model [1]. To ensure comparability of outcomes, our study adopts analogous parameters and design variables as employed by Filippi.

The aeroelastic wing model has seven design variables, see Figure 1, where s denotes the semi-wingspan, x_f is the coordinate of the flexural axis measured from the nose, m is the unit mass per area of the wing, c is the chor length, x_cm is the position of the center of gravity, K_κ and K_θ are the flapping and pitching stiffnesses. x_cm and x_f are normalized with the chord. The design

parameters are arranged into a vector,

$$x_{\mathrm{d,struct}} = \begin{bmatrix} s & c & m & K_\kappa & K_\theta & x_{\mathrm{cm}} & x_{\mathrm{f}} \end{bmatrix}^T. \tag{1}$$

The rectangular wing has two rotational springs at the root to provide flap κ and pitch θ degrees of freedom. There is no stiffness coupling between the torsional and bending motions [8]. Table 1 contains the fixed parameters of the model for the equation of motion.

Table 1: Parameters of the simplified wing model

Notation	Name	Value
ρ	Density	$1.225\,\mathrm{kg/m^3}$
V	Air speed	$100\ \mathrm{m/s}$
a_{w}	Lift curve slope	2π
$M_{\dot{\theta}}$	Unsteady aero damping term	-1.2

A Lagrangian equation is formulated for the semi-span of the wing. On the right-hand side, the equation incorporates both the deflection of the control surface, denoted as β, and the influence of external factors such as wind gusts or turbulence, encapsulated by the term w_g. The open-loop system has the following form

$$\tilde{A}\ddot{q} + \rho V \tilde{B}\dot{q} + (\rho V^2 \tilde{C} + \tilde{E})q = g\beta + hw_{\mathrm{g}}, \tag{2}$$

where $\tilde{A}$ is the structural inertia, $\tilde{B}$ is the aerodynamic damping, $\tilde{C}$ and $\tilde{E}$ are the aerodynamic stiffness and structural stiffness matrices. The generalized coordinates vector contains the flapping and pitching angles $q = \begin{bmatrix} \kappa \\ \theta \end{bmatrix}$. The value of the matrices in Equation 2 are

$$\begin{aligned}
\tilde{A} &= \begin{bmatrix} I_\kappa & I_{\kappa,\theta} \\ I_{\kappa,\theta} & I_\theta \end{bmatrix}, & \tilde{B} &= \begin{bmatrix} \frac{cs^3 a_{\mathrm{w}}}{6} & 0 \\ -\frac{ec^2 s^2 a_{\mathrm{w}}}{4} & -\frac{c^3 s}{8} M_{\dot{\theta}} \end{bmatrix}, \\
\tilde{C} &= \begin{bmatrix} 0 & \frac{cs^2 a_{\mathrm{w}}}{4} \\ 0 & -\frac{ec^2 s a_{\mathrm{w}}}{2} \end{bmatrix}, & \tilde{E} &= \begin{bmatrix} K_\kappa & 0 \\ 0 & K_\theta \end{bmatrix}, \\
g &= \begin{bmatrix} g_1 \\ g_2 \end{bmatrix} = c\rho v^2 s \begin{bmatrix} \frac{-sa_{\mathrm{c}}}{4} \\ \frac{cb_{\mathrm{c}}}{2} \end{bmatrix}, & h &= \begin{bmatrix} h_1 \\ h_2 \end{bmatrix} = c\rho V s \begin{bmatrix} \frac{-s}{4} \\ \frac{c}{4} \end{bmatrix}.
\end{aligned} \tag{3}$$

In these matrices, I_{ij} is the inertia, e is the eccentricity between the flexural axis and the aero center, K_i is the stiffness, $a_{\mathrm{c}}, b_{\mathrm{c}}$ are a function of a_{w} and the fraction of chord made up by control surface. The eccentricity is determined as

$$e = \frac{x_{\mathrm{f}}}{c} - 0.25. \tag{4}$$

The stiffness is calculated from the flapping (f_κ) and pitching (f_θ) frequencies

$$K_i = (2\pi f_i)^2 I_{ii}, \tag{5}$$

where $i = \kappa, \theta$. The $a_{\mathrm{c}}, b_{\mathrm{c}}$ functions are formulated as

$$a_{\mathrm{c}} = \frac{a_{\mathrm{w}}}{\pi}(\cos^{-1}(1 - 2EE) + 2\sqrt{EE(1 - EE)}), \tag{6}$$

$$b_{\mathrm{c}} = -\frac{a_{\mathrm{w}}}{\pi}(1 - EE)\sqrt{EE(1 - EE)}), \tag{7}$$

where $EE = 0.1$ constant, denotes the fraction of chord taken up by control surface. The Equation 2 is rearranged into a first-order state space system as,

$$\begin{bmatrix}\dot{q}\\ \ddot{q}\end{bmatrix} = \begin{bmatrix}0 & I\\ -\tilde{A}^{-1}(\rho V^2\tilde{C}+\tilde{E}) & -\tilde{A}^{-1}(\rho V\tilde{B})\end{bmatrix}\begin{bmatrix}q\\ \dot{q}\end{bmatrix} + \begin{bmatrix}0\\ \tilde{A}^{-1}g\end{bmatrix}\beta + \begin{bmatrix}0\\ \tilde{A}^{-1}h\end{bmatrix}w_g. \tag{8}$$

This is of the form:

$$\dot{x} = Ax + Bu + Hd. \tag{9}$$

where x are the generalized coordinates, the input is the control surface deflection angle β, and the wind disturbance w_{g},

$$x = \begin{bmatrix}q\\ \dot{q}\end{bmatrix} = \begin{bmatrix}\kappa\\ \theta\\ \dot{\kappa}\\ \dot{\theta}\end{bmatrix}, \qquad u = \beta, \qquad d = w_g. \tag{10}$$

The output equations, referred to as virtual sensor signals, are computed despite the absence of physical sensors on the wing. Instead, precise values are calculated, which correspond to the hypothetical sensor locations. One challenge arises during the computation of virtual sensor accelerations due to the state variables are angular quantities. To solve this, a conversion matrix is required, incorporating geometric parameters of the wing such as the semi-span (s), flexural axis position from the wing's leading edge (x_f), and chord length (c). The conversion matrix T is defined as follows:

$$\begin{bmatrix}a_1\\ a_2\end{bmatrix} = T\begin{bmatrix}\ddot{\kappa}\\ \ddot{\theta}\end{bmatrix} \qquad \text{, where} \qquad T = \begin{bmatrix}s & x_{\mathrm{f}}\\ s & c - x_{\mathrm{f}}\end{bmatrix}. \tag{11}$$

The state-space equations need displacement values in absolute terms. Therefore, we require an extension to convert angular outputs into displacement outputs for calculation,

$$C = \begin{bmatrix}T & 0 & 0\\ 0 & T & 0\\ 0 & 0 & T\end{bmatrix}_{6x6}\begin{bmatrix}I_{4x4}\\ -\tilde{A}^{-1}(\rho V^2\tilde{C}+\tilde{E}) & -\tilde{A}^{-1}(\rho V\tilde{B})\end{bmatrix}_{6x4}, \tag{12}$$

$$D = \begin{bmatrix}T & 0 & 0\\ 0 & T & 0\\ 0 & 0 & T\end{bmatrix}_{6x6}\begin{bmatrix}0 & 0\\ B & H\end{bmatrix}_{6x2}. \tag{13}$$

The state space is expressed in the following simplified form:

$$\dot{x} = Ax + [B\ H]\begin{bmatrix}u\\ d\end{bmatrix}, \tag{14}$$

$$y = Cx + D\begin{bmatrix}u\\ d\end{bmatrix}. \tag{15}$$

The outputs are $y = [x_1,\ x_2,\ v_1,\ v_2,\ a_1,\ a_2]$, which are displacement values and its derivatives.

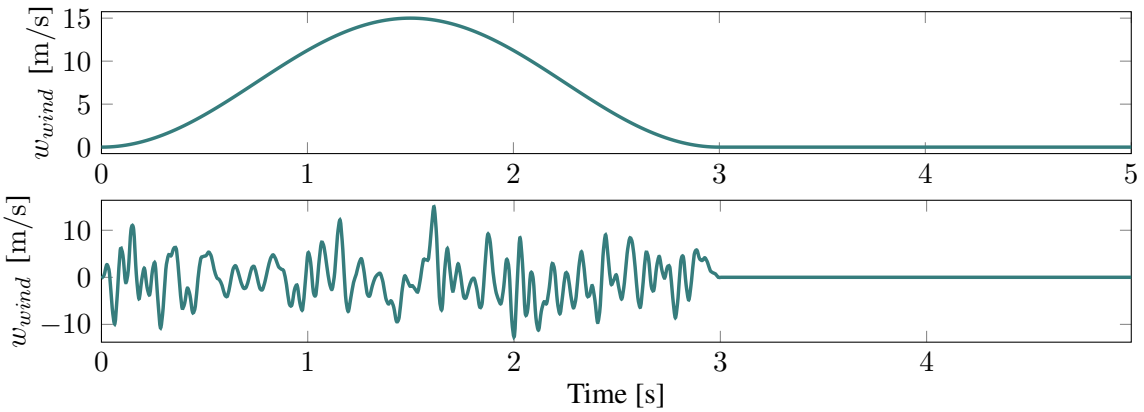

Figure 2: Turbulence and *1 - cosine* vertical wind gusts for time domain simulations

2.1 Wind disturbances

The flexible wing model contains the turbulent and the 1-cosine excitations in the d term of Equation 9. The wind gust disturbs the system dynamics, forcing the open-loop system into instability. The used disturbances are presented in Figure 2. Typically, these gusts manifest in an upward direction. As they buffet the aeroelastic wing, they augment the bending and twisting forces on the wings. Consequently, this alteration in behavior can propel the aircraft into instable zones where flutter occurs. There are two main categories of gusts to consider: discrete gusts, which follow a predictable pattern, often in a shape of a 1-cosine function, and continuous turbulence, characterized by random fluctuations in gust velocity. Vertical gusts notably influence the aircraft's pitch and heave motions, with the wind gust velocity presumed to remain uniform across the span of the wing [9]. In the flexible wing model, turbulent and 1-cosine disturbances are incorporated into the *d* term in Equation 9.

3 CONTROL METHODOLOGY

This section describes the designing of a controller. For flutter suppression control, we use acceleration and anglular velocity sensors because these are commonly found on aircrafts. These sensors are placed at the free tip of the wing model, because this is where the most noticeable changes can be observed. We use two control scenarios to mitigate flutter, the first one is PI control with acceleration sensors, and the second one is PID control with angular velocity measurements. The control gains are optimization variables in the co-design framework.

3.1 PI Control

The first control scenario employs acceleration signals alongside PI control. Two acceleration sensors, positioned at the wingtip corners as illustrated by blue dots in Figure 1, are necessary to detect both bending and torsion rates. These sensors enable us to identify both symmetric and asymmetric wing movements. By integrating the acceleration sensor signals, we obtain the velocity response of the wing. The definition of the error term is the following,

$$\underline{e}(t) = \begin{bmatrix} v_{1,\text{ref}} \\ v_{2,\text{ref}} \\ a_{1,\text{ref}} \\ a_{2,\text{ref}} \end{bmatrix} - \begin{bmatrix} v_1(t) \\ v_2(t) \\ a_1(t) \\ a_2(t) \end{bmatrix}. \tag{16}$$

where the v_1 velocity and a_1 acceleration are determined at the leading-edge corner of the wing, and v_2 velocity and a_2 acceleration are at the trailing-edge wingtip corner. The reference values

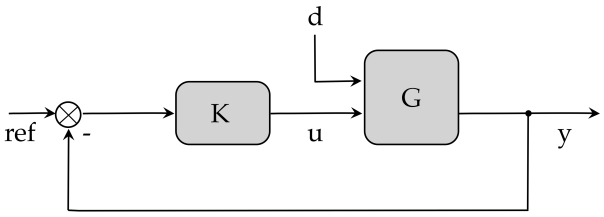

Figure 3: The closed control loop

are zeros because the aim is to eliminate all kinds of oscillations in the system and prove as smooth flying as possible. The PI controller is of the form of

$$u_{\text{act}} = P_1 \cdot e_3 + P_2 \cdot e_4 + \frac{1}{s}\left(I_1 \cdot e_3 + I_2 \cdot e_4\right) = P_1 \cdot e_3 + P_2 \cdot e_4 + I_1 \cdot e_1 + I_2 \cdot e_2 \tag{17}$$

Bandwidth contrstraints posed by the actuator are taken into account as follows.

$$W_{\text{act}} = \frac{\omega_{\text{n}}^2}{s^2 + 2\zeta\omega_{\text{n}}s + \omega_{\text{n}}^2}. \tag{18}$$

Our actuator dynamics definitions adopt a second-order transfer function characterized by the angular frequency ω_{n} and damping ratio ζ. The bandwidth for the actuator is set at $f = 100\,\text{Hz}$, i.e. $\omega_{\text{n}} = 2\pi f = 628\,\frac{\text{rad}}{\text{s}}$, and its damping ratio of $\zeta = 1$ employed in the simulation. The actuator's output signal corresponds to the deflection of the control surface, symbolized as β. This angular displacement, denoted as u in Equation 9, serves as the input parameter for the aeroelastic system.

3.2 PID Control

The second control scenario incorporates angular speed feedback along with its integral and derivative terms. Although the output equations in state-space form remain consistent with the previous setup, the conversion matrix is omitted due to the direct feedback of angular quantities. The same actuator characteristics is applied, where the actuator output is the control surface deflection angle β. The PID controller has a form as,

$$u_{\text{act}} = P_1 \cdot e_3 + P_2 \cdot e_4 + \frac{1}{s}\left(I_1 \cdot e_3 + I_2 \cdot e_4\right) + s\left(I_1 \cdot e_3 + I_2 \cdot e_4\right) \tag{19}$$

$$= P_1 \cdot e_3 + P_2 \cdot e_4 + I_1 \cdot e_1 + I_2 \cdot e_2 + D_1 \cdot e_5 + D_2 \cdot e_6 \tag{20}$$

Figure 3 illustrates the closed-loop system. For the derivation of the closed-loop transfer function in our scenario, the following procedure can be employed.

$$W_{\text{closed-loop}} = \frac{W_{\text{open}}}{1 + W_{\text{open}}}, \tag{21}$$

where the open-loop is the product of the transfer functions of the controller weights W_{c}, actuator W_{act} and aeroelastic system W_{sys}

$$W_{\text{open}} = W_{\text{c}} \cdot W_{\text{act}} \cdot W_{\text{sys}}. \tag{22}$$

The calculations are implemented in Matlab, where the `feedback()` function can be used to create the closed-loop system from the open-loop form.

Table 2: Upper and lower bounds of the design variables

Design variable	Lower Bound	Upper Bound
s	$3\,\mathrm{m}$	$15\,\mathrm{m}$
$x_{\mathrm{f},\%}$	0.35	0.9
m	$70\,kg$	$130\,\mathrm{kg}$
$x_{\mathrm{cm},\%}$	0.1	0.9
f_κ	$3\,\mathrm{Hz}$	$9\,\mathrm{Hz}$
f_θ	$5\,\mathrm{Hz}$	$15\,\mathrm{Hz}$
P_1	-100	100
P_2	-100	100
I_1	-100	100
I_2	-100	100
D_1	-100	100
D_2	-100	100

4 OPTIMIZATION SETUP

In preparation for optimizing the simplified wing, the initial step involves defining a suitable cost function to assess the optimization task effectively. This cost function should accurately reflect the objectives to yield a meaningful optimum. Our control-wing design relies on a comprehensive cost function that incorporates handling, comfort, and control expenses. The cost function is formulated as follows:

$$J = \int_0^T \left(w_1 z^2 + w_2 \ddot{z}^2 + w_3 u^2\right) \mathrm{d}t, \tag{23}$$

where z represents the vertical displacements measured at the wingtip edges, and the weights $w_1 = 10^3$, $w_2 = 10^{-2}$, and $w_3 = 10^2$ ensure uniform magnitude across each component of the objective function. The overall cost function comprises the sum of objectives related to turbulence and *1-cosine* gusts.

$$J = J_{\cos} + J_{\mathrm{turb}}, \tag{24}$$

where $J_{\cos}$ and J_{turb} are the evaluated integrals in Equation 23. The cost function is the same as Filippi reported so that it can give a representative comparison between the results [1].

The constraints play a crucial role in bounding the optimization process, ensuring that iterations remain within physically realistic parameters. The wing area is constrained to a constant value $S = c{\cdot}s = 15\ \mathrm{m}^2$,where c represents the chord and s denotes the semi-span width. Additionally, the eccentricity between the flexural axis and the aerodynamic center is bounded within $0.1 < e < 1$. Furthermore, the maximum allowable vertical displacement is limited to $|z| < 1\ \mathrm{m}$. The design variables are constrained by both lower and upper bounds. The optimization process is confined within this range of values. Table 2 provides a summary of the lower and upper bounds associated with each design variable. In cases where only proportional-integral (PI) control is employed, the derivative (D) terms are excluded from the control process.

We use MATLAB for optimization. Specifically, we use the `fmincon` function to find the minimum of a constrained nonlinear function. Our approach employs the Sequential Quadratic Programming (SQP) algorithm, which offers two key advantages. Firstly, SQP does not require starting from a feasible point, making it easier to use with nonlinear constraints. Secondly,

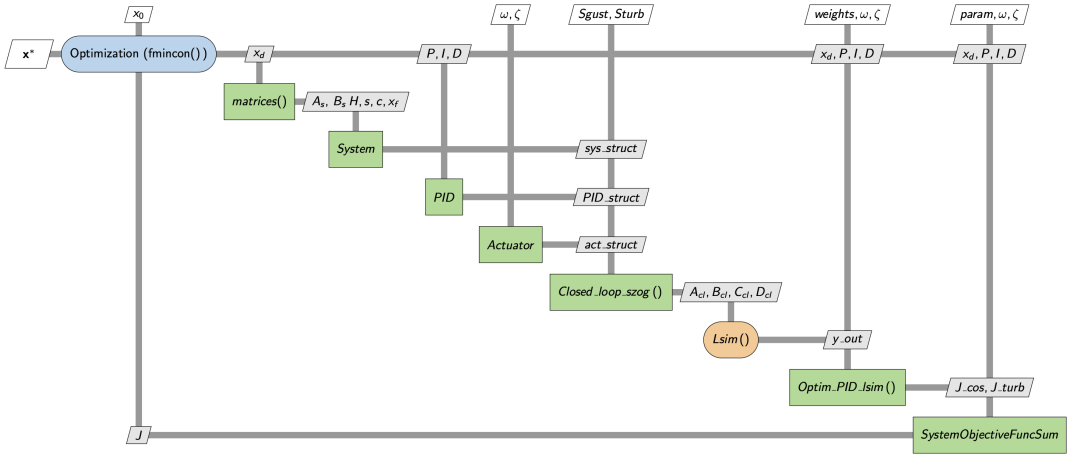

Figure 4: Extended design structure of the co-design problem of the wing

SQP relies on fast and accurate algorithms, particularly suitable for solving quadratic programs. When only equality constraints are present, the solution simplifies to solving a linear system of equations [10]. The algorithm is categorized as medium-scale, necessitating full matrix storage in memory. Although it exhibits improved performance, its computational demands are higher compared to those of large-scale problems. Nevertheless, given the nature of our problem, the SQP algorithm is deemed a suitable choice.

The computation of the cost function gradient is non-trivial. To address this, `fmincon()` approximates the gradient. We adopt the central finite difference scheme due to its ability to offer richer information and better estimation. Despite its drawback of doubling the number of function evaluations compared to the forward differencing scheme, it can significantly reduce the iteration count under specific tolerances, thereby potentially offering computational cost advantages. The Extended Design Structure Matrix is created for the problem to present the optimization process, according to reference [11]. In Figure 26, the architecture of the problem is depicted. The functions have been developed within the MATLAB environment. Here, we aim to provide a concise overview of the operational methodology employed in the optimization process.

The `fmincon()` function is initialized with the initial design variable guess, x_0, and subsequently constructs system matrices based on the provided design variables. In the first iteration, `fmincon()` supplies the initial design variable guess, and the system matrices are defined according to Equation 8. PID guesses and actuator dynamics are then formulated as per Equation 18. The closed-loop components are computed to construct the state-space model of the closed-loop system, as depicted in Equation 21, enabling system behavior simulation. The simulation is executed using the `lsim()` built-in function, yielding the time response of the closed-loop system for specified outputs. The cost function, formulated according to Equation 23, is then compiled, leading to the calculation of the objective value J. This value serves as input for `fmincon()`, where the Sequential Quadratic Programming (SQP) algorithm iteratively refines the solution. Upon meeting predefined criteria, the process halts, delivering the optimized solution x^*.

Table 3: Optimized design variables for acceleration feedback

s	$x_{\mathrm{f},\%}$	m	$x_{\mathrm{cm},\%}$	f_κ	f_θ	P_1	P_2	I_1	I_2	J
15 m	0.5	130 kg	0.5	9 Hz	10.9261 Hz	-0.0355	15.9236	-0.7493	-50.6	1.560922

Table 4: Optimized design variables for angular velocity feedback

s	$x_{\mathrm{f},\%}$	m	$x_{\mathrm{cm},\%}$	f_κ	f_θ	P_1	P_2	I_1	I_2	D_1	D_2	J
7.792 m	0.5	70 kg	0.5	4.574 Hz	5.025 Hz	-70.181	-8.68	-1.56	-0.21	-1.20	-0.147	0.8817

5 RESULTS

In this section, we present the optimization results. Initially, we discuss the optimization outcomes of the controller using acceleration sensors, followed by the controller utilizing angular velocity sensors. Subsequently, we will compare these results with Filippi's initial model.

The optimized design variables for PI control are summarized in Table 3. A few notable observations can be drawn from the results. Firstly, the variable s, representing half the wing span, attains the upper bound of the design space, suggesting a preference for larger aspect ratios by the optimizer. Moreover, maximizing the wing's weight proves advantageous in terms of comfort cost considerations. Additionally, asymmetry between the two acceleration sensors induced by the wing's torsional motion is evident from the different signs of the proportional P gains. Furthermore, there is a notable disparity in the magnitude of the integral gain. Eliminating torsional motion contributes to a more efficient cost function. The values of the cost function J are listed in the last column of the table.

The optimized design parameters for angular velocity feedback control are outlined in Table 4. Upon analysis, it is observed that the semi-wing span length deviates from prior configurations, residing midway between upper and lower bounds. This adjustment is accompanied by a reduction in wing weight, thereby enhancing maneuverability. Notably, the PID gains exhibit slight asymmetry. Evaluation of the cost function reveals a significantly diminished value compared to acceleration feedback control, indicative of superior efficiency in angular velocity feedback control within our specific context. This finding aligns with similar conclusions drawn by Patartics et al. [4], wherein angular feedback control outperforms acceleration feedback.

Figure 5 illustrates the outcomes of angular velocity feedback control and the acceleration feedback contol. Both time responses are stable, so the optimization can stabilize the system by the cost function minimization. After the disturbance ends (starting from the 3rd second), there are fewer oscillations in the responses, indicating quicker stabilization. Notably, both the control input angle and displacement magnitudes are reduced compared to the acceleration feedback-based control. The larger wingspan resulting from acceleration feedback leads to larger wingtip displacements. Furthermore, the displacements at the wingtip exhibit synchronous behavior for both control scenrarios, see Figure 6, indicating effective suppression of torsional motions by the controller. An important distinction with angular velocity feedback is that PID gains are associated with angular movements, allowing for post-time response analysis to derive position and acceleration properties via a transformation matrix.

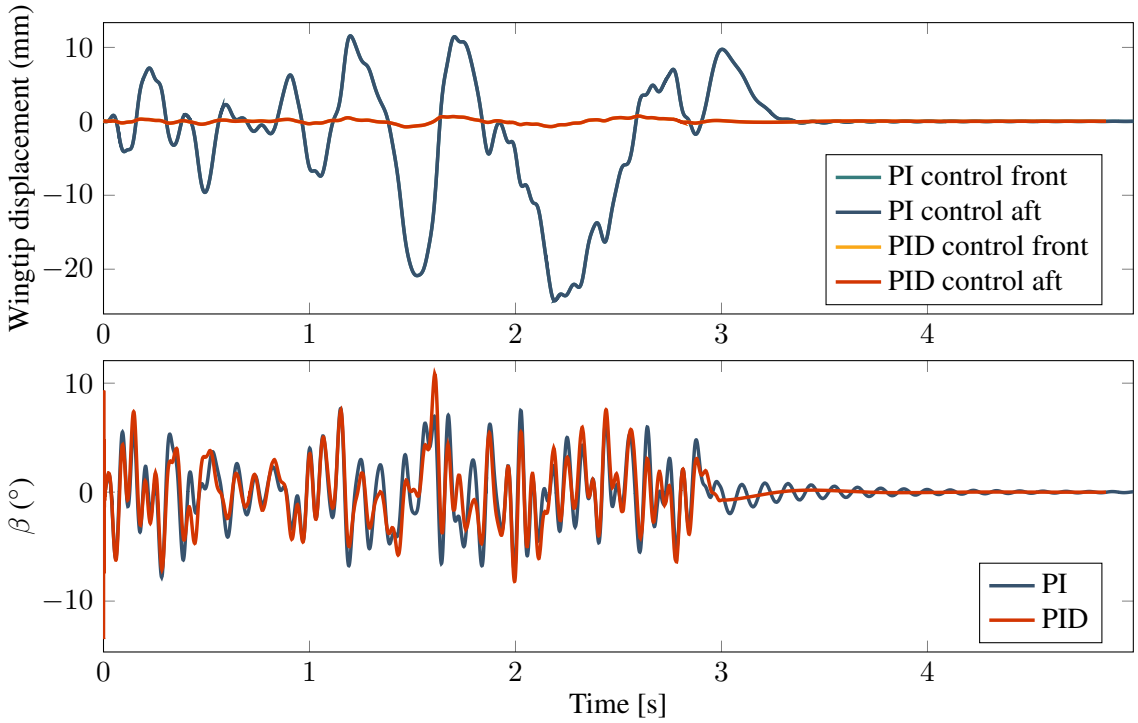

Figure 5: Comparison of the acceleration feedback and angluar feedback results

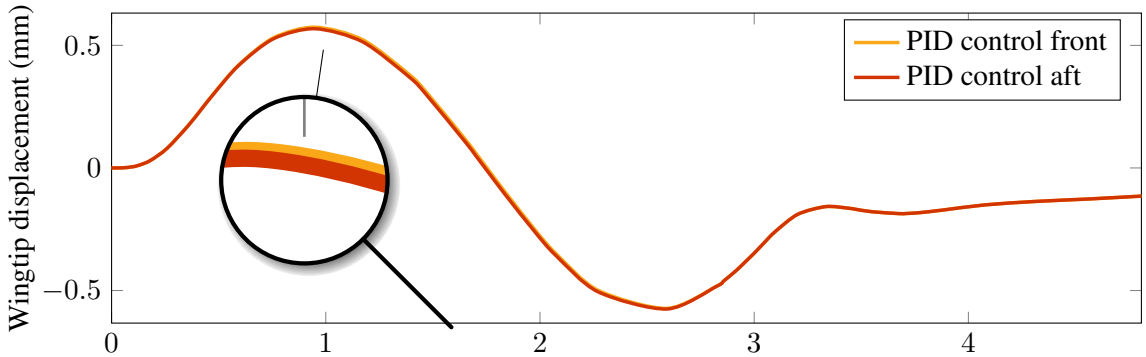

Figure 6: The front and the aft of the wing at the wingtip are synchronized, thus the torsional motion of the wing is suppressed.

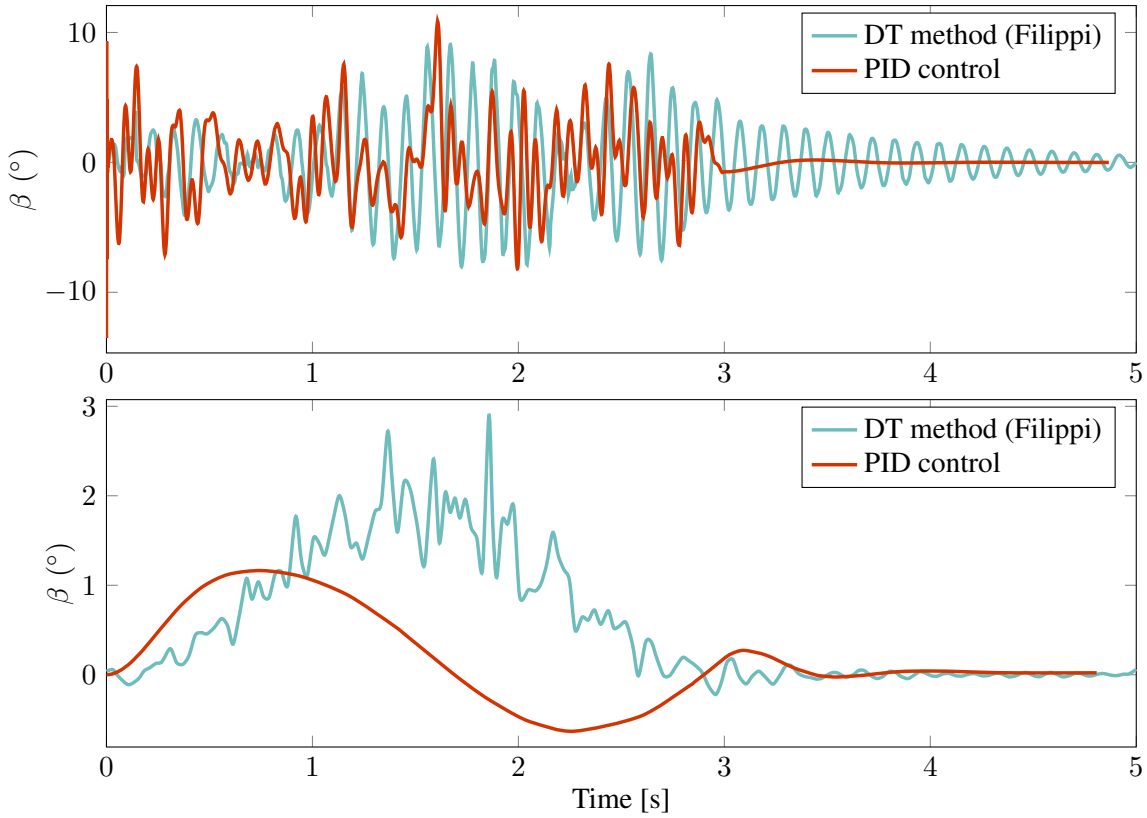

Figure 7: Comparison of the control surface angles between Direct Transcription and feedback control methods

Table 5: Cost values comparison

$J_{\text{min,Filippi}}$	$J_{\text{min,cl}}$	Reduction (%)
4.67	0.8817	81.11%

For comparative analysis with the initial model, we employ the optimized solution derived from angular feedback control. Filippi's findings are publicly accessible via a GitHub repository [1]. In Figure 7, control input angles are presented for comparative analysis. Figure 8 illustrate wingtip displacements under different disturbances. Bluish lines depict Filippi's results incorporating optimized control inputs, while the redish line represents our implementation of control inputs from the optimized PID controller. Each plot illustrates that the closed-loop results exhibit significantly reduced oscillations compared to Filippi's optimal results. In Filippi's theoretical optimization investigation, the torsional mode exhibits a greater influence than feedback control, thereby explaining the divergent wingtip positions depicted in Figure 8. Comparison of the cost functions is presented in Table 5. Given the similarity in cost functions, they serve as reliable indicators for result comparison. Implementation of a straightforward PID feedback controller yields a substantial 81.11% reduction in the cost value, signifying a significant enhancement in efficiency. The optimized values fall within a realizable range, offering a feasible solution.

6 CONCLUSION

In conclusion, the utilization of Multidisciplinary Design Optimization (MDO) presents notable challenges in controlling and structurally designing aeroelastic wings. Directly applying MDO to real models requires caution due to the inherent complexity of the system. However, contemporary research trends support the increasing adoption of MDO frameworks in the structural, aerodynamic, and control design disciplines.

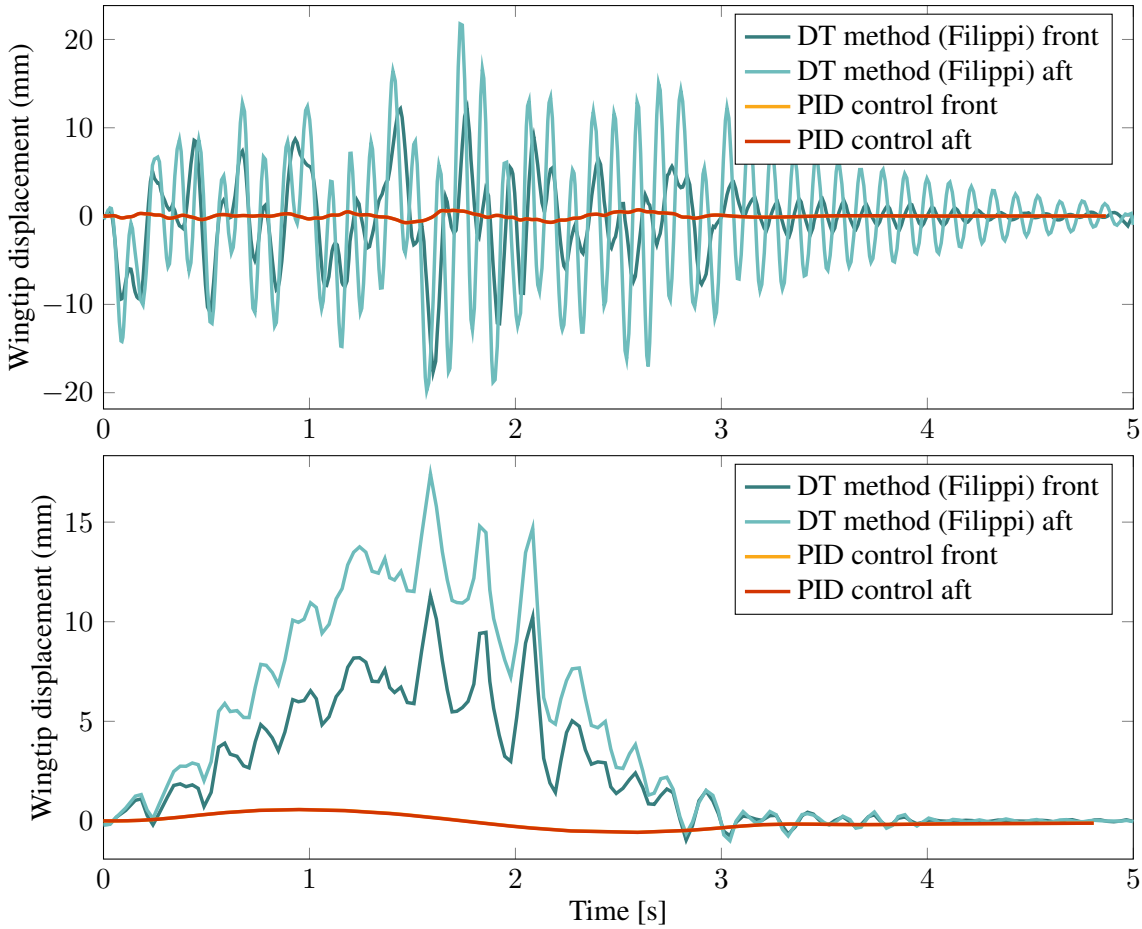

Figure 8: Turbulence and *1 - cosine* wind gusts for time domain simulations

Filippi's work introduces a 'state-of-art' concept by optimizing structural parameters based on an aeroelastic model subject to wind gust perturbations using Direct Transcription method. This approach acknowledges the critical influence of aeroelastic modes on aircraft stability, particularly the flutter mode, which can induce instability. The optimization process targets a stable system with negative poles, which is a fundamental but not trivial assumption. In contrast, our approach emphasizes practicality by integrating wing sensors to establish input-output relationships and designing controllers alongside structured design considerations for aeroelastic stability. However, it is important to note that feedback mechanisms alone do not ensure system stability, which warrants fine-tuning of controllers. The optimization process solves this tuning through a well-designed cost function.

Our study aims to validate Filippi's theoretical model while extending it with practical controls, thereby improving the understanding of the multidisciplinary design optimization (MDO) process. By experimenting with Proportional Integral (PI) and Proportional Integral Derivative (PID) controllers, which incorporate feedback from different sensor signals, we aimed to optimize system performance. Applying feedback based on angular velocity allowed an impressive 81.11% improvement in the cost function compared to Filippi's results and effectively reduced the flutter phenomenon. It is encouraging that our results show a significant improvement of the cost function, confirming the potential of our method.

7 REFERENCES

[1] Filippi, G. and Morlier, J. (2018). Integrated structural and control system design for robust flutter performance. *ISAE-SUPAERO Institut Suprieur de l'Aronautique et de l'Espace*. Avalaible at: `https://github.com/mid2SUPAERO/PIR_Giovanni_Filippi_FlutterMDO`, Downloaded: 2024.05.20.

[2] Livne, E. (2018). Aircraft Active Flutter Suppression: State of the Art and Technology Maturation Needs. *Journal of Aircraft*, 55(1), 410–452. ISSN 0021-8669, 1533-3868. doi:10.2514/1.C034442.

[3] Theis, J., Pfifer, H., and Seiler, P. J. (2016). Robust Control Design for Active Flutter Suppression. In *AIAA Atmospheric Flight Mechanics Conference*. San Diego, California, USA: American Institute of Aeronautics and Astronautics. ISBN 978-1-62410-390-2. doi:10.2514/6.2016-1751.

[4] Patartics, B., Liptak, G., Luspay, T., et al. (2022). Application of Structured Robust Synthesis for Flexible Aircraft Flutter Suppression. *IEEE Trans. Contr. Syst. Technol.*, 30(1), 311–325. ISSN 1063-6536, 1558-0865, 2374-0159. doi:10.1109/TCST.2021.3066096.

[5] Denieul, Y., Bordeneuve-Guibé, J., Alazard, D., et al. (2017). Integrated design of flight control surfaces and laws for new aircraft configurations. *IFAC-PapersOnLine*, 50(1), 14180–14187. ISSN 24058963. doi:10.1016/j.ifacol.2017.08.2085.

[6] Faïsse, E., Vernay, R., Vetrano, F., et al. (2021). Adding Control in Multidisciplinary Design Optimization of a Wing for Active Flutter Suppression. In *AIAA Scitech 2021 Forum*. Virtual event: American Institute of Aeronautics and Astronautics. ISBN 978-1-62410-609-5. doi:10.2514/6.2021-0892.

[7] Nguyen, N. T., Ting, E., and Lebofsky, S. (2016). Inertial Force Coupling to Nonlinear Aeroelasticity of Flexible Wing Aircraft. In *15th Dynamics Specialists Conference*. San Diego, California, USA: American Institute of Aeronautics and Astronautics. ISBN 978-1-62410-398-8. doi:10.2514/6.2016-1094.

[8] Wright, J. and Cooper, J. (2008). *Introduction to Aircraft Aeroelasticity and Loads*. Aerospace Series. Wiley. ISBN 978-0-470-85846-2.

[9] Khodaparast, H. H. and Georgiou, G. (2013). Efficient Worst Case "1-Cosine" Gust Loads Prediction. *Journal of Aeroelasticity and Structural Dynamics*, (3), 33–54. ISSN 1974-5117. doi:10.3293/asdj.2012.17.

[10] Boggs, P. T. and Tolle, J. W. (1996). Sequential Quadratic Programming. *Acta Numerica*, 52.

[11] Lambe, A. B. and Martins, J. R. R. A. (2012). Extensions to the design structure matrix for the description of multidisciplinary design, analysis, and optimization processes. *Structural and Multidisciplinary Optimization*, 46, 273–284. doi:10.1007/s00158-012-0763-y.